Materials Today Advances 14 (2022) 100238

Contents lists available at ScienceDirect

Materials Today Advances

journal homepage: www.journals.elsevier.com/materials-today-advances/

Three-dimensional highway-like graphite flakes/carbon fiber hybrid electrode for electrochemical biosensor

Y. Yu [a, **], C. Jiang [a], X.T. Zheng [a], Y. Liu [a, d], W.P. Goh [a], R.H.H. Lim [b], S.C.L. Tan [a], L. Yang [a, c, *]

[a] Institute of Materials Research and Engineering, The Agency for Science, Technology and Research (A*STAR), 2 Fusionopolis Way, #08-03, Innovis, 138634, Singapore
[b] Singapore Institute of Technology, 10 Dover Dr, 138683, Singapore
[c] Department of Materials Science and Engineering, College of Design and Engineering, 9 Engineering Drive 1, National University of Singapore, 117575, Singapore
[d] Department of Biomedical Engineering, College of Design and Engineering, 4 Engineering Drive 3, National University of Singapore, 117583, Singapore

ARTICLE INFO

Article history:
Received 23 January 2022
Received in revised form
15 March 2022
Accepted 22 March 2022
Available online xxx

Keywords:
Flexible electrochemical sensor
Amperometric detection
Screen-printed carbon electrode
Hybrid material
Carbon fiber
Prussian blue

ABSTRACT

Carbon-based electrodes are promising candidates for developing cheap, miniaturized, and disposable biosensors for effective, point-of-care disease management. However, their sensitivity is usually lower than gold electrodes due to polymer binders used during the procedure of ink formulating. Although surface pretreatment with reactive chemicals and addition of nanomaterials are available to enhance their sensor performance, both approaches may suffer from the use of hazardous substances and processing complexity. Here, we report an inexpensive, non-nanomaterials approach by making a graphite/carbon fiber (G/CF) hybrid electrode for biosensor applications. The hybrid electrode is formed by embedding a homemade graphite ink in the CF matrix of a commercially available carbon paper. This design resembles a super-efficient 3D highway network where ample expressways (CF) run through numerous small factories (locally distributed graphite flakes) for rapid goods pick-up and transportation (electron transfer). Featuring high conductivity, low impedance and large active surface area surpassing commercial screen-printed carbon electrodes, the G/CF hybrid electrodes show superior sensor performance for glucose detection as compared to counterparts prepared on electrodes without CF matrix. This study provides a new approach of enhancing electrochemical performance of carbon-based electrodes by structural design using macro-size scale, affordable materials.

1. Introduction

Electrochemical biosensors are key for real-time point-of-care monitoring of biological levels of a specific marker for effective disease management [1–4]. An electrochemical biosensor probes and quantifies a certain biomarker, e.g. ions, drugs, or molecular metabolites, by measuring an electrical signal proportional to the concentration of the given biomarker [5]. A typical electrochemical biosensor has three electrodes, namely working electrode (W.E.), reference electrode (R.E.), and counter electrode (C.E.), which are patterned on a solid planar substrate [6]. The electrochemical event of interest occurs on the W.E. which is usually made from carbon, gold or silver materials. Carbon-based (graphite, carbon black, or active carbon) electrodes are advantageous due to their low cost, being operational on a broad potential window, being chemically inert, and easy mass production by well-established printing techniques [7,8]. They are most promising for developing cheap, miniaturized, disposable biosensors.

Conventionally, carbon-based electrodes come with intrinsic shortcomings as compared to gold electrodes. As carbon materials used for electrode fabrications are free of functional groups, a considerable amount of polymer binder is needed during the procedure of formulating carbon ink/paste, which cannot be totally removed and finally retards electron transfer for sensing. Sluggish electron transfer is amplified for enzyme-based biosensors as the active sites of an enzyme are usually buried deep in its pocket. Much work has been done to improve the sensor performance of carbon-based electrodes. One possible way to improve the electron transfer of carbon-based electrodes is via surface pretreatment

* Corresponding author.
** Corresponding author.
E-mail addresses: yuy@imre.a-star.edu.sg (Y. Yu), yang_le@imre.a-star.edu.sg (L. Yang).

https://doi.org/10.1016/j.mtadv.2022.100238

using chemicals like hydrogen peroxide, sulfuric acid, or ozone to remove excessive binders [9,10]. However, such pretreatment usually involves reactive hazards and increases the complexity of sensor fabrication. Besides pretreatments, tremendous efforts have also focused on using certain nanomaterials, such as gold nanoparticles [11], carbon nanotubes [12], carbon nanofibers [13], or two-dimensional materials (e.g., graphene, molybdenum disulfide) [14], to modify the carbon electrode by providing wiring effect [15] for better electron transfer. The sensor properties such as the linear range of detection and sensitivity have been largely improved. However, these nanomaterials are expensive and poor in reproducibility. The ongoing debate on potential adverse health effects of nanomaterials is another concern worth noting [16,17]. More importantly, such nanomaterials are usually discretely distributed only on the surface of the electrode, by which the improvement in electron transfer may be limited. If a three-dimensional (3D) network structure for electron transfer can be implemented, the electrochemical performance of the resultant electrode can be greatly enhanced.

We present here a unique design of three-dimensional (3D) highway-like graphite/carbon fiber (G/CF) hybrid electrode, in which graphite flakes from a homemade graphite-based ink are embedded into a 3D carbon fiber framework. In this unique hybrid structure, carbon fibers of several micrometers in diameter (in contrast to carbon nanofibers) serve as channels for fast transfer of electrons generated from redox reactions at the local graphite particles, much resembling a 3D highway system running through numerous scattered factories to provide avenues for rapid goods pick-up and transportation. In addition, the carbon fiber can also reinforce the graphite-based electrode by holding the graphite flakes together and increase the porosity and surface area of the resulting hybrid electrode. We utilize a commercially available carbon paper (CP) for the 3D CF framework, which has high electrical conductivity, high mechanical strength, and high chemical resistance. The structure and electrochemical performance of the fabricated hybrid electrode were examined by scanning electron microscopy (SEM), X-ray photoelectron spectroscopy (XPS), cyclic voltammetry (CV), and electrochemical impedance spectroscopy (EIS). We evaluate the sensor performance of the hybrid electrode by functionalizing it with glucose oxidase (GOx) as catalyst and Prussian blue (PB) as mediator, for glucose detection. Effects of preparation method and loading amount of PB on the sensor performance have also been studied. Presented below are details of this investigation.

2. Materials and methods

2.1. Chemicals and instruments

Iron(III) chloride ($FeCl_3$), potassium ferricyanide ($K_3[Fe(CN)_6]$), potassium chloride (KCl), acetic acid (CH_3COOH), hydrochloric acid (HCl), chitosan from shrimp shells (≥75%, deacetylated), bovine serum albumin (BSA), glucose oxidase (type VII from *Aspergillus niger*), polyvinylpyrrolidone (PVP) were purchased from Merck. All chemicals were used as received.

Cyclic voltammetry (CV) and real-time amperometric detection were performed on a μStat 8000 Multi Potentiostat/Galvanostat from DropSens. Electrochemical impedance spectroscopy (EIS) measurements were done on a PalmSens4 Potentiostat. X-ray photoelectron spectroscopy (XPS) measurements were obtained on a PHI Quantera SXM Scanning XPS Microprobe. Scanning electron microscopy (SEM) images were recorded on a JEOL JSM6700F field emission scanning electron microscope operating at 5 kV. UV—vis spectra were recorded on a Shimadzu UV-2450 spectrometer.

2.2. Fabrication of graphite/carbon fiber hybrid electrode

A three-electrode configuration consisting of a rectangular-shaped working electrode (W.E.) and counter electrode (C.E.) was adopted for the graphite/carbon fiber (G/CF) hybrid electrode (Fig. 1). Both the areas of W.E. and C.E. are 0.1 cm^2. The key component of the electrode is a graphite/carbon fiber hybrid material, which was prepared by coating a homemade graphite-based paste/ink onto a carbon paper sheet (29AA, SGL Carbon) using blade coating method and dried at 80 °C for 5 min. The graphite-based paste was prepared by mixing 3 g of graphite (Timcal Timrex KS6), 6 g of poly(3,4-ethylenedioxythiophene) polystyrene sulfonate (PEDOT:PSS) (Heraeus Clevios PH1000) and 6 mg of polyvinylpyrrolidone (PVP) in a Thinky planetary Mixer at 2000 rpm for 5 min. PEDOT:PSS was introduced as a polymer binder to promote the dispersion of graphite flakes and the adhesion of ink to the substrate. A small amount of PVP was used to adjust the hydrophilicity of the graphite-based ink. The coating and drying process was repeated multiple times if necessary to vary the loading of graphite ink on the carbon paper. After being heated at 130 °C for 10 min, the G/CF hybrid was cut into the shape of the W.E. and C.E. and attached on a polyimide (PI) substrate. A silver paste (Dycotec SIP−3061S) was then printed using an ink dispenser to define three silver lines with one as the reference electrode (R.E.) while the other two connected to the W.E. and C.E., respectively. The printed Ag lines were heated at 130 °C for 10 min. Finally, a dielectric layer (DuPont 5036) was printed using the ink dispenser to mask the unnecessary surfaces. The printed dielectric layer was heated at 130 °C for 5 min.

2.3. Fabrication of glucose sensor with the G/CF electrode

The glucose sensor is based on the enzymatic oxidation of glucose and constructed by using glucose oxidase (GOx) as the catalyst and Prussian blue (PB) as the mediator. Briefly, PB particles were first loaded onto the G/CF electrode, followed by coating a thin layer of GOx on the PB modified electrode. Two different approaches were used to make the PB layer. In the first approach, PB nanoparticles were prepared by a reductant induced precipitation method according to a reported method [18]. The synthesized PB nanoparticles were washed with 0.1 M KCl/0.1 M HCl and re-dispersed to desired concentrations based on its optical density. 5 μL of the re-dispersed PB solutions at different concentrations were dropcast on the W.E. and dried in a 4 °C refrigerator overnight. The second approach involved coating a PB layer on the G/CF W.E. via electrochemical deposition. A mixture solution of $FeCl_3$ (2.5×10^{-3} M) and $K_3[Fe(CN)_6]$ (2.5×10^{-3} M) dissolved in 0.1 M KCl/0.1 M HCl (50 μL) was applied to cover the entire three electrodes and swept from −0.2 to 0.6 V at 0.05 V/s for various different (2, 5, 10) cycles. The excess solution was carefully drawn after CV scanning. The G/CF electrodes modified with electrochemically deposited PB were also dried at 4 °C overnight. The enzyme solution was prepared by mixing solutions of GOx (50 g/L with 10 g/L BSA in phosphate buffered saline) and chitosan (1 wt% in 2 wt% acetic acid) in 1:1 vol ratio [19]. 3 μL of the enzyme mixture solution was cast on the G/CF electrodes modified with either dropcast or electrochemically deposited PB, and dried at 4 °C overnight prior to sensor performance tests.

3. Results and discussion

The electrochemical performance of the typical G/CF hybrid electrode is first examined by cyclic voltammetry using the Fe^{3+}/Fe^{2+} redox couple (Fig. 2a). The anodic and cathodic peaks appear rather symmetric and bell-shaped, suggesting the charge transfer

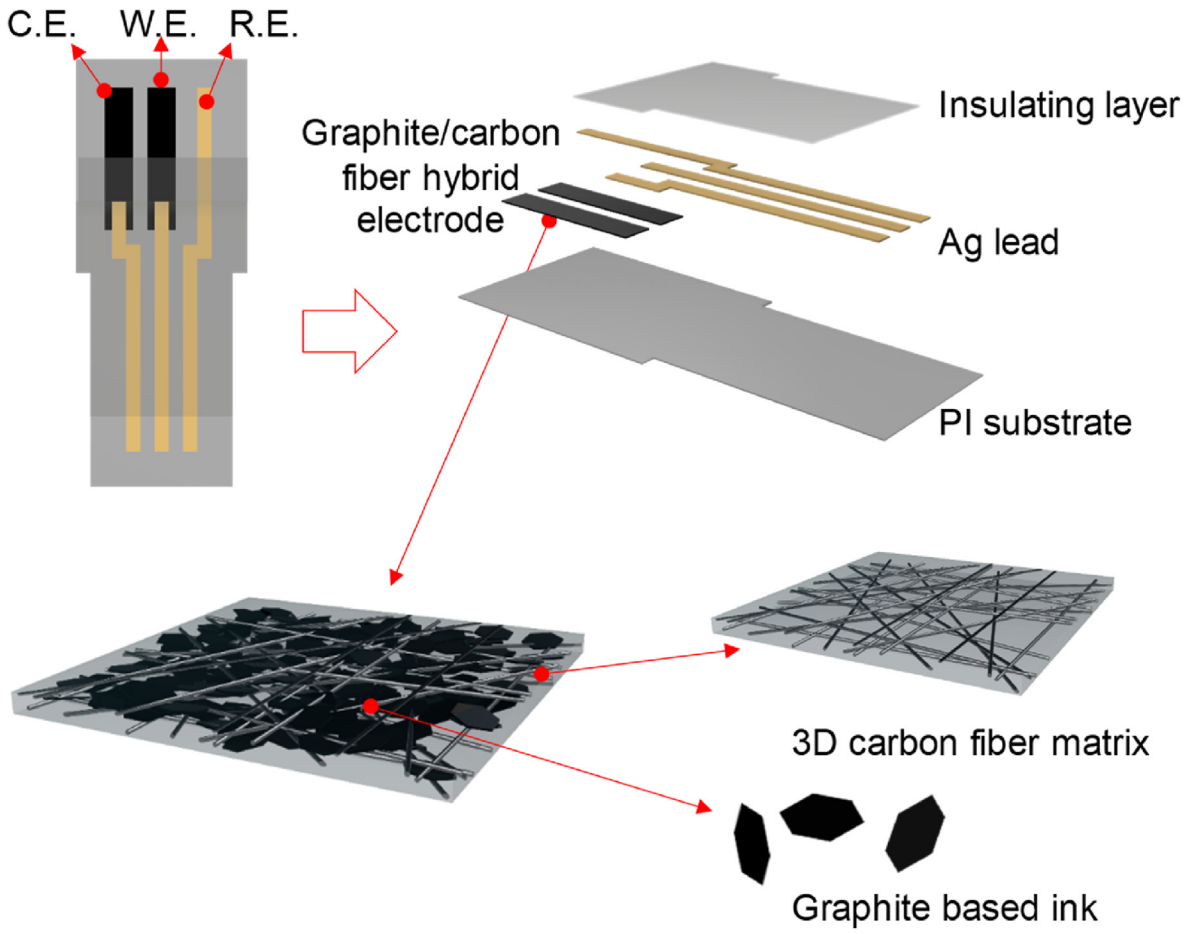

Fig. 1. Schematic illustration of the three-dimensional highway-like graphite/carbon fiber (G/CF) hybrid electrode adopting a three-electrode configuration.

process is reversible and the electrochemically active species are well immobilized on the electrode. The half-height widths of both anodic and cathodic peaks are ~0.108 V, close to the theoretical value of ~0.091 V predicted from the Nernstian equation for a one-electron redox couple immobilized on the electrode at room temperature [20]. The peak current ratio (i_{pA}/i_{pC}) is close to 1 throughout all the scan rates studied, which also confirms the reversibility of the charge transfer process (Fig. S1). Moreover, the anodic and cathodic peak currents are quite high, confirming the high conductivity of the G/CF electrode thanks to the carbon fibers in the CP framework. In comparison, the current densities of commercial screen-printed carbon electrodes are only 1/3 to 1/2 that of the G/CF electrode (Fig. S2 and Table S1). In addition, we observe the peak currents to be more linearly correlated to the scan rate than the square root of scan rate (Fig. 2b and Fig. S3), suggesting the electrochemical process is more kinetic-controlled than diffusion-controlled. The surface concentration of the electrochemical active species can be calculated according to the following equation [21].

$$i_p = \frac{n^2F^2A\Gamma v}{4RT} \quad (1)$$

where i_p is the anodic or cathodic peak current, n is number of electrons transferred for the chosen redox couple, F is the Faraday constant, Γ is surface coverage, v is scan rate in V/s, R is the universal gas constant, and T is absolute temperature. Based on the slopes of the fitted straight lines, the adsorbed Fe^{2+} and Fe^{3+} on the electrode are calculated to be 5.79×10^{-8} and 5.75×10^{-8} mol/cm^2 respectively. This result agrees well with the high surface area of the G/CF electrode due to its micro-porosity formed by packing of graphite particles. The high surface area of the G/CF electrode has been also validated by the relative active surface area estimated from the CV results according to the Randles-Sevčik equation [22].

$$i_p = 2.69 \times 10^5 n^{3/2} A D^{1/2} C v^{1/2} \quad (2)$$

where D is the diffusion coefficient constant and C is the bulk concentration of the electrochemically active species, while the other symbols are defined in Equation (1). The relative active surface area of G/CF electrode is 230.7%, which is 3–4 times that of a commercial screen-printed carbon electrode (Table S1).

We further investigate the G/CF electrode by electrochemical impedance spectroscopy (EIS). The resultant Nyquist plot shows the property of an electric double-layer capacitor (EDLC), attributed to three major parts (Fig. 2c) [23]. At high frequency, the internal resistance is the sum of electrode resistance and electrolyte resistance (**a**), and is found to be rather small (~10 Ω). At middle frequency region, the diffusion resistance is due to double-layer build-up (**b**), while the last region is the equilibrium differential capacitance (**c**). We then adopt a modified Randle's equivalent circuit model (Fig. 2d inset) to fit the Bode plot to better reflect the frequency-dependent response (Fig. 2d). The double-layer capacitance is calculated from the fitting for the G/CF electrode and compared with commercial screen-printed carbon electrode on PET substrate. The double-layer capacitance of G/CF electrode

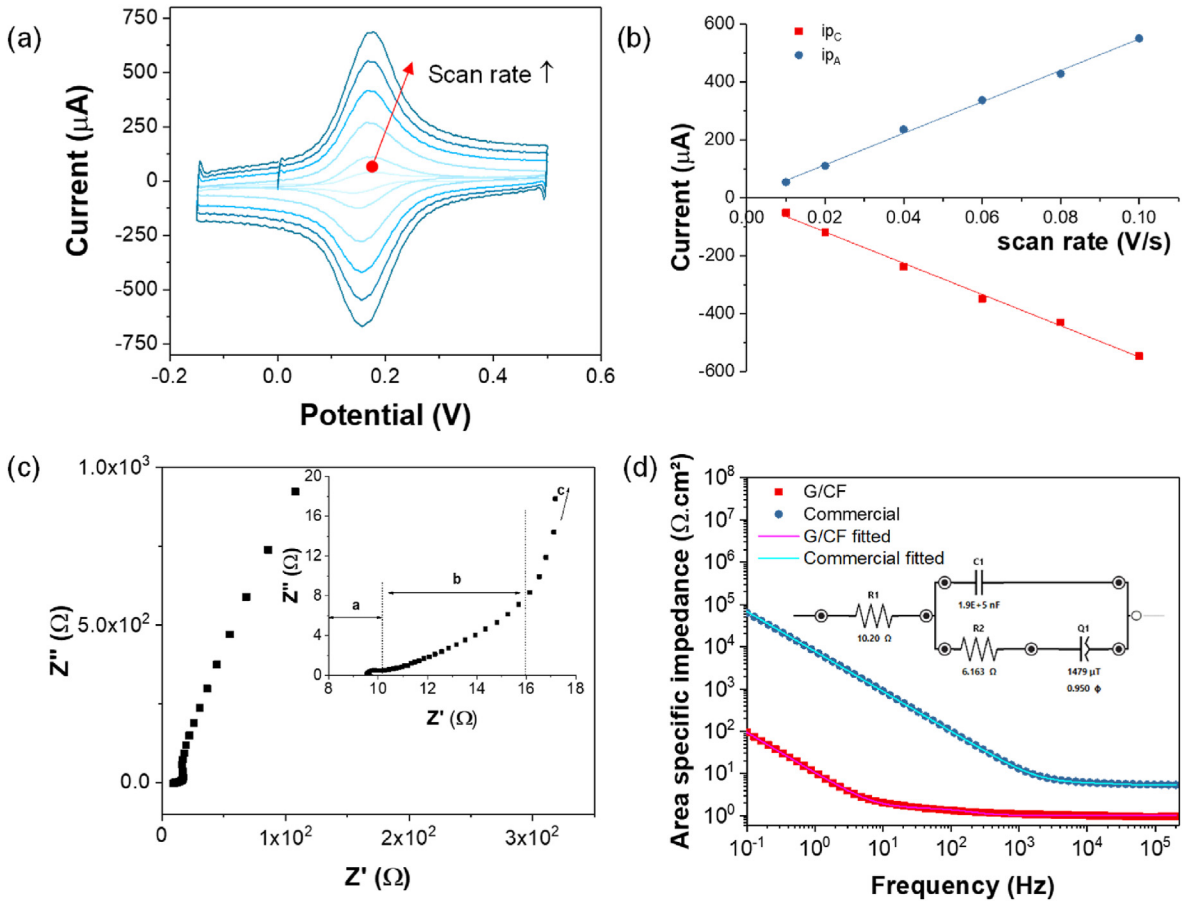

Fig. 2. (a) Cyclic voltammograms of the G/CF electrode in 5×10^{-3} M ferricyanide solution at different scan rates (0.01, 0.02, 0.04, 0.06, 0.08, and 0.1 V/s from innermost, light-blue, to outermost, dark-blue). (b) Plots of i_{pC} and i_{pA} against the scan rate. (c) Nyquist plot and (d) Bode plot of the G/CF electrode measured in 10×10^{-3} M PBS. (Inset of c) Zoomed-in Nyquist plot at the medium-to-high frequency region. (Inset of d) Equivalent circuit model of the G/CF electrode for EIS simulation. Bode plot of a commercial electrode (Lan Printech, Part No. LP-3.12D1. WP.350) measured at the same experiment condition is also included for comparison.

(1.9 mF/cm^2) is substantially higher than that of the commercial electrode (5.7 μF/cm^2), owing to its volumetric capacitance and high porosity. Because of the ultrahigh double-layer capacitance of G/CF electrode, the area-specific impedance of G/CF is ~3 orders of magnitude lower than that of the commercial electrode at low frequency of 0.1 Hz, and ~1/6 that of the commercial electrode at high frequency of 10^5 Hz. A low impedance electrode is favorable for rapid current flow, allowing for increased detection sensitivity [24].

The amount of graphite ink loaded on the carbon paper (i.e., graphite ink-to-CP weight ratio) is critical in determining the structure and electrochemical performance of the G/CF hybrid electrode. Fig. 3 shows the schematic illustrations (row a) and corresponding SEM images (row b and c) of carbon paper loaded with varying amount of graphite ink (loading increases from left to right). When no graphite ink is loaded (graphite ink-to-CP ratio of 0, the first column), the CP alone features a macro-porous structure with a pore diameter of several hundred micrometers, which is constructed by lots of carbon fibers of ~7 μm in diameter crossing over each other. It should be mentioned some graphite coating already exists in the carbon paper as received (row b, the first column). Nevertheless, large hollow pores can be observed across the entire carbon paper. The SEM image of the cross-section shows the carbon paper has a hollow interior and its overall thickness is 235.6 ± 1.0 μm (row c, the first column). The corresponding CV curve (Fig. S4a) is not well-defined even for a model Fe^{3+}/Fe^{2+} redox couple and has a low current density. As the loading of graphite ink slightly increases to a moderate value (e.g., graphite ink-to-CP ratio of 0.36, the second column), the large pores of carbon paper are gradually filled with small graphite flakes (with a particle size of 3–5 μm) to make a more solid structure (row b, the second column). However, some cracks are still observed due to a low packing density of graphite particles. The interior still adopts a hollow structure, and the overall thickness decreases slightly to 219.6 ± 2.0 μm possibly due to pressing during blade coating (row c, the second column). The obtained peak current density in CV scan (Fig. S4b) is high but does not adopt a well-defined shape, which could be due to the poor stability of the electrode linked with the cracks. When the loading of graphite ink reaches the other extreme (e.g., graphite ink-to-CP ratio of 2.42, the last column), excessive graphite ink starts to form an additional (purely graphite-based) layer over the carbon paper after all the pores have been filled (represented by the shadow from the top view and the top layer from the side view). The surface of the hybrid appears smooth (row b, the last column). However, the cross-section view shows a two-tier structure with a denser upper layer (row c, the last column). The overall thickness of the hybrid material in this scenario is 264.2 ± 3.8 μm. The CV curve also shows a large double layer capacitance because of this two-tier structure (Fig. S4d). Both the top view and cross-section SEM images confirm the uniform structure of the G/CF hybrid with an optimal loading at a moderate graphite-to-CP ratio (e.g., 1.64, the third column), which allows all

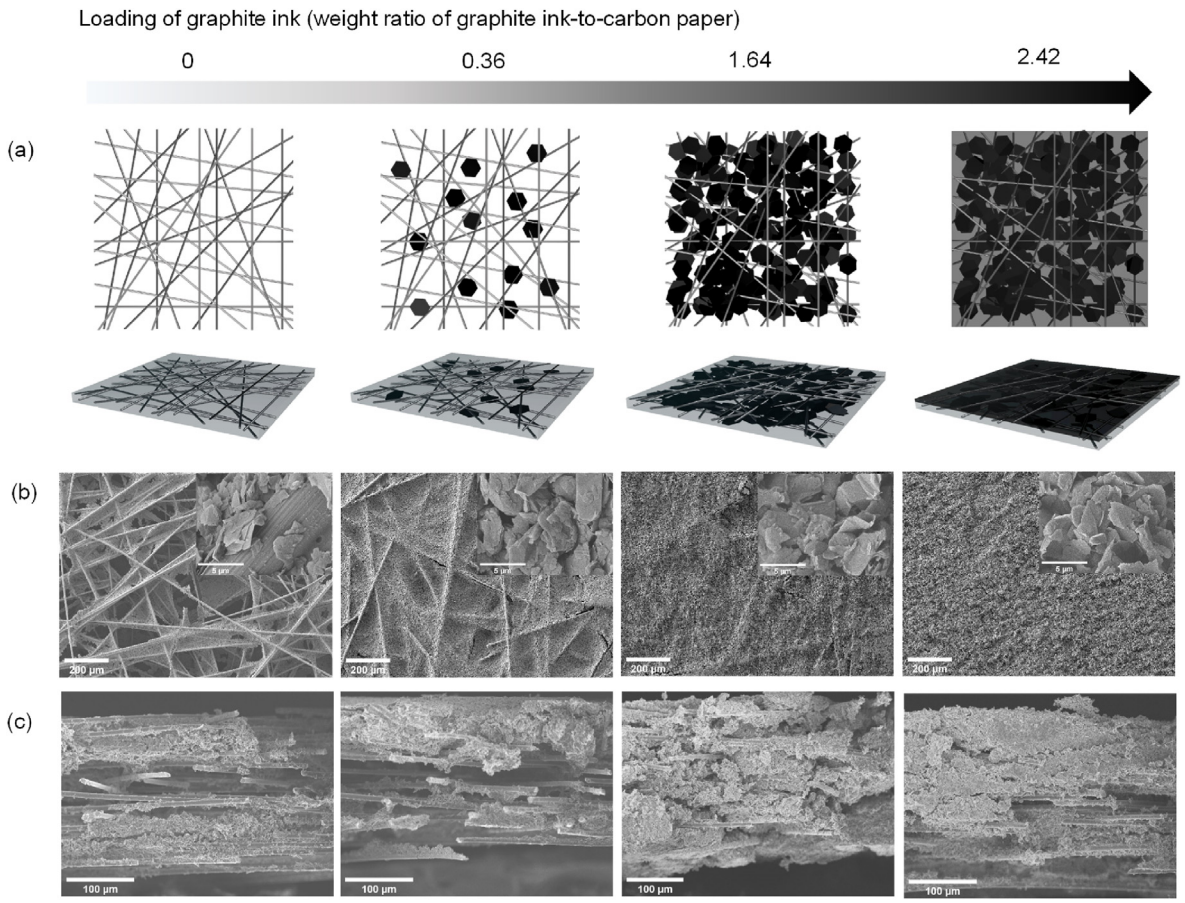

Fig. 3. (a) Schematic illustration of the top view and side view (rod – carbon fibers, hexagon – graphite ink), (b and c) SEM images of the top view and side view (cross-section) of the G/CF hybrid electrodes with varied weight ratios of graphite ink-to-CP (0–2.42 from left to right). The scale bar of inset figures in b is 5 μm.

the large pores of the carbon paper to be just filled with graphite ink, yet no second graphite ink layer is formed on top of the CF matrix. The overall thickness of the optimal G/CF hybrid is 300.2 ± 5.5 μm. Besides the SEM images, we also conduct XPS analysis to confirm the proposed structures of the G/CF hybrid with varied graphite ink loadings. Three peaks (284.78 eV for C–C, 285.52 eV for C–O, and 290.22 eV for π-π* transition) have been identified on the de-convoluted high resolution C1s spectrum of the carbon paper (Fig. S5). An additional peak at ~287 eV appears when graphite ink starts to load into the CF matrix. This peak is attributed to C=O due to the interaction of PEDOT:PSS contained in the graphite ink (as binder) with the CF matrix [25]. Moreover, the contribution of this peak increases from an estimated 0–15%, agreeing well with the relative graphite ink:CF (*vide supra*).

Next, we demonstrate the biosensor application of the G/CF electrode by detecting glucose as a model example. Glucose is a biomarker for diabetes, one of the most prevalent chronic diseases [3]. The prevailing electrochemical sensor for glucose relies on the enzymatic oxidation of glucose using glucose oxidase (GOx) due to its high sensitivity and specificity. Here, we fabricate the flexible glucose sensor by coating a thin layer of GOx on a G/CF hybrid W.E. and using Prussian blue (PB) particles as an electron mediator. PB deposition on the G/CF electrode has been optimized for sensor performance in two approaches. In the first approach, PB nanoparticles prepared by a reported method [18] were dropcast on the W.E. before modifying with GOx. The aqueous solution of the PB nanoparticles shows a broad absorption peak at ~700 nm (Fig. S6), whose optical density can determine the PB concentration [26]. The amount of PB loaded on the G/CF W.E. was then varied (0.1–0.25 nmol) to optimize the glucose sensor.

Fig. 4a is a typical SEM image of the glucose sensor modified with 0.15 nmol PB by dropcasting (dPB). The red arrows point out several PB particles in lumps that are distinct from the neighboring flake-shaped graphite particles. These PB particles, being a few micrometers in size, are aggregates of the primary nanometer-sized PB particles due to their high surface energy. XPS further corroborates the presence of PB (Fig. 4c), where all its elements can be found in the survey spectrum. The $Fe2p_{3/2}$ and $Fe2p_{1/2}$ peaks are seen at 708 and 720.5 eV, respectively. The CV curve of the flexible glucose sensor modified with dPB determines its optimal amperometric working potential (Fig. S7). A slight decrease in peak current is observed at 0 V upon glucose addition, which confirms the electron-accepting effect of the PB mediator. Glucose sensing of is thus performed at 0 V for the dPB modified sensors. The non-polarized detection of glucose by amperometry is an additional bonus of the current design to minimize interferences of other biomolecules usually associated with an applied voltage. Fig. 4e summarizes the performance of dPB-modified flexible glucose sensors. All sensors with different amount of dPB show a good sensitivity (17.8–24.5 μA mM^{-1} cm^{-2}) and wide linear response range (0–1.28 mM) that well covers the physiological level of glucose in sweat [3], as these flexible electrodes are potential candidates for on-skin wearable sensors. The limit of detection (LOD) of the optimized glucose sensor is estimated to be 64.7 μM based on a signal-to-noise ratio of 3. The sensitivity of a flexible glucose sensor prepared similarly on an electrode without CF is

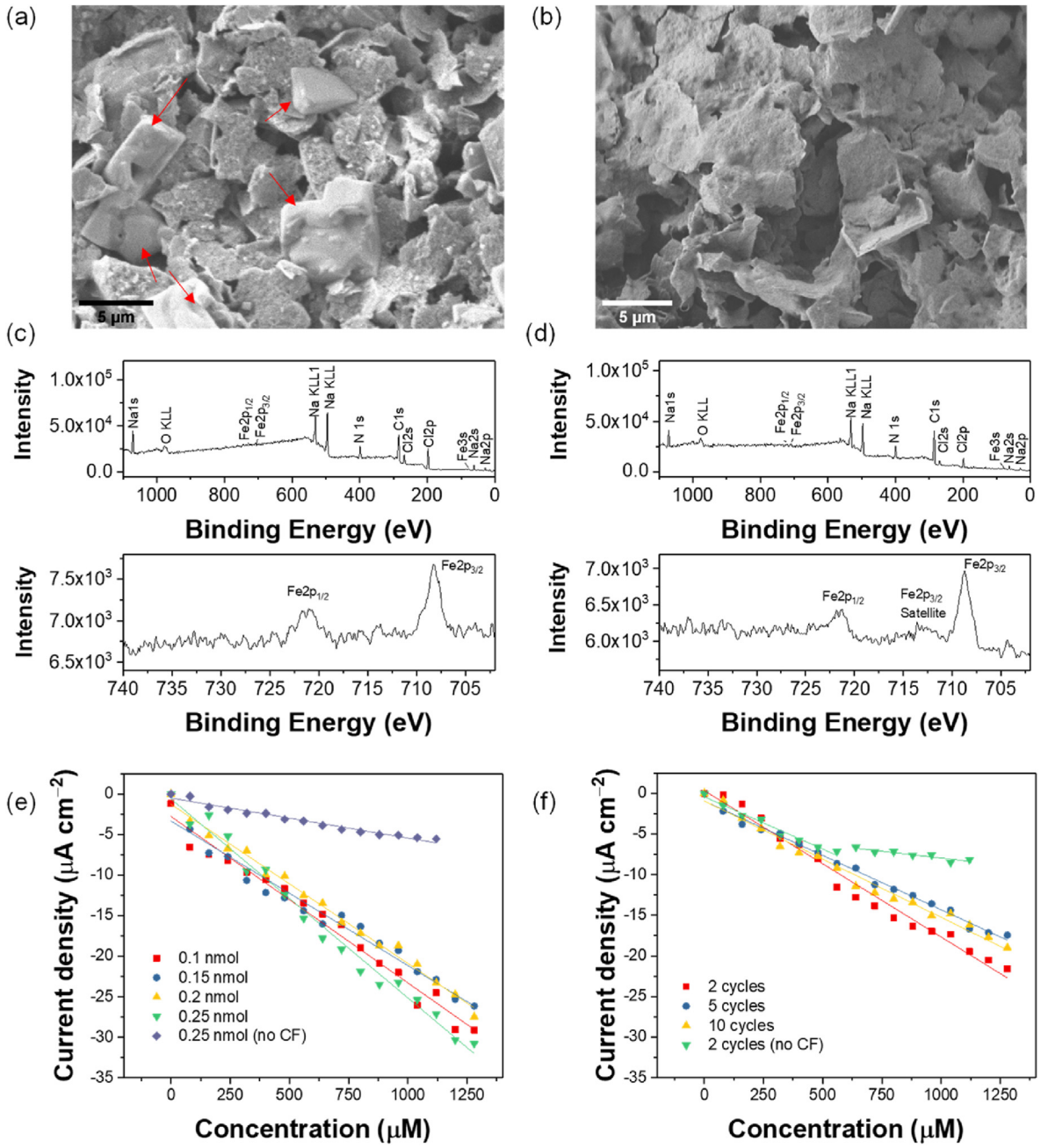

Fig. 4. (a, b) SEM images of glucose sensor made on (a) G/CF electrode dropcast with pre-synthesized PB particles or dPB (indicated by red arrows) and (b) G/CF electrode with electrochemically deposited PB or ePB (scanned for 2 cycles). (c, d) XPS survey spectra (top) and Fe2p spectra (bottom) of glucose sensor using (c) dPB and (d) ePB as mediator. (e, f) Plots of current density against the glucose concentration for electrodes modified with (e) various amount of dPB (■ 0.1 nmol ● 0.15 nmol ▲ 0.2 nmol ▼ 0.25 nmol) and their linear regression results (solid lines), and (f) ePB prepared at different cycles (■ 2 ● 5 ▲ 10 cycles) and their linear regression results (solid lines). The results tested on an electrode with graphite ink only were also included for comparison (♦0.25 nmol, no CF in e and ▼ 2 cycles, no CF in f), respectively.

only 4.9 μA mM^{-1} cm^{-2}, which further reinforces the advantages of the G/CF hybrid design - its porous structure, high surface area, good conductivity, and network effect.

In the second approach, the PB mediator has been prepared on G/CF electrodes by electrochemical deposition (ePB). CV scans of various cycles (2, 5, and 10 cycles) were applied to deposit PB from a mixture solution of iron chloride and ferricyanide (Fig. S8). Unlike the dropcasting approach, CV scans lead to a different surface with larger pores and the deposited PB can be barely observed (Fig. 4b). Nevertheless, the presence of ePB is verified by XPS analysis (Fig. 4d). We observe an additional satellite peak from the high-resolution spectrum of Fe2p attributable to the high pin state of Fe^{3+} from the oxidative conversion of initially-formed PB [27]. The optimal potential used for amperometric glucose detection using the ePB flexible glucose sensor has been determined to be 0.1 V by CV (Fig. S9). Fig. 4f summarizes the performance of flexible glucose sensors prepared with ePB-modified G/CF electrodes. The sensor with ePB formed by scanning 2 cycles exhibits the highest sensitivity (18.0 μA mM^{-1} cm^{-2}), consistent with a previous report that ePB formed by fewer cycles of CV scan has a higher sensitivity [1].

The sensitivities of all three ePB-modified sensors (18.0, 13.4, and 14.3 μA mM^{-1} cm^{-2} for ePB formed by scanning 2, 5 and 10 cycles, respectively) are lower than those modified with dPB, suggesting dropcasting of preformed PB is a better to way to fabricate PB-mediated enzymatic sensors on graphite-based electrodes with a high porosity. Despite the lower sensitivity, the ePB-modified glucose sensors show a wide linear working range like the dPB-modified ones (up to 1.28 mM). In contrast, the sensors prepared without CF show both a poorer sensitivity (12.9 μA mM^{-1} cm^{-2}) and a much narrower linear response range (0–560 μM) despite the ePB preparation conditions being the same, again confirming the enhancement from the unique structure of G/CF electrode for biosensor applications.

Lastly, we have compared the electroanalytical performance of our best glucose sensors (e.g, 0.25 nmol dPB modified G/CF hybrid electrodes) with those reported in literature (Table S2). Our glucose sensors have shown respectable same-batch reproducibility with RSD of 7% (n = 3) and can retain nearly 50% of its initial sensitivity after being stored in ambient atmosphere at 4 °C for 2 weeks. The linear response range (0–1.28 mM), sensitivity (up to 24.5 μA mM^{-1} cm^{-2}), and LOD (64.7 μM) of our sensors are decent and comparable to reported enzyme-based glucose sensors on screen-printed carbon electrodes, and well cover the biological range of sweat glucose [3]. In addition, our glucose sensors also show good specificity against common biomolecules such as cysteine, uric acid and urea (Fig. S10). Testing on artificial sweat samples, we are able to obtain a high recovery (96.4%) when spiked with known concentrations of glucose, indicating promising sweat sensor applications of our G/CF electrodes.

4. Conclusions

In summary, we present here a unique graphite/carbon fiber (G/CF) hybrid electrode designed for electrochemical biosensor applications. The hybrid electrode is constructed by embedding a homemade graphite ink in the CF matrix of a commercially available carbon paper. The as-designed G/CF electrode much resembles a 3D highway system in which the CF matrix serves as expressways to channel the rapid transfer of electrons generated at the local graphite particle “factories”. Characterizations of the G/CF hybrid electrodes by SEM, XPS, CV, and EIS highlight the importance of the 3D CF matrix of the CP, which not only provides a framework for holding the graphite ink, but also renders the resulting electrode with excellent conductivity, low impedance, high porosity, and large active surface area. The distinct structural features of the G/CF hybrid electrodes translate well into enhanced biosensor applications. As a model demonstration, glucose sensors fabricated on the G/CF hybrid electrodes show decent sensitivities (up to 24.5 μA mM^{-1} cm^{-2}), limit of detection (64.7 μM) and wide linear response ranges (0–1.28 mM) as compared with graphite-only electrodes without CF matrix. The PB formation process and loading amount of PB mediator have also been carefully investigated, which suggest dropcasting pre-synthesized PB nanoparticles (dPB) is a better option than electrochemical deposition (ePB) to achieve superior sensor performance on such highly porous graphite-based electrodes. Our work forms a precursor to developing flexible wearable electronics.

Credit author statement

Yong Yu: Conceptualization, Investigation, Methodology, Data curation, Visualization, Writing – original draft. Changyun Jiang: Conceptualization, Methodology, Writing – review & editing. Xin Ting Zheng: Methodology, Writing – review & editing. Yuxin Liu: Methodology, Writing – review & editing. Wei Peng Goh: Writing – review & editing. Roger Hui Heng Lim: Methodology. Sherwin Chong Li Tan: Writing – review & editing. Le Yang: Supervision, Discussion, Writing – review & editing.

Declaration of competing interest

The authors declare that they have no known competing financial interests or personal relationships that could have appeared to influence the work reported in this paper.

Acknowledgements

This work was supported by A*STAR AME Programmatic Funds under grant A18A1b0045, and the A*STAR Central Research Fund. The authors thank Mr. Jia Jie Gan for schematic drawings and Ms. Huiqing Xie for XPS analysis.

Appendix A. Supplementary data

Supplementary data to this article can be found online at https://doi.org/10.1016/j.mtadv.2022.100238.

References

[1] W. Gao, S. Emaminejad, H.Y.Y. Nyein, S. Challa, K. Chen, A. Peck, H.M. Fahad, H. Ota, H. Shiraki, D. Kiriya, D.-H. Lien, G.A. Brooks, R.W. Davis, A. Javey, Nature 529 (2016) 509–514, https://doi.org/10.1038/nature16521.
[2] H. Lee, T.K. Choi, Y.B. Lee, H.R. Cho, R. Ghaffari, L. Wang, H.J. Choi, T.D. Chung, N. Lu, T. Hyeon, S.H. Choi, D.-H. Kim, Nat. Nanotechnol. 11 (2016) 566–572, https://doi.org/10.1038/nnano.2016.38.
[3] H. Lee, C. Song, Y.S. Hong, M.S. Kim, H.R. Cho, T. Kang, K. Shin, S.H. Choi, T. Hyeon, D.-H. Kim, Sci. Adv. 3 (2017), e1601314, https://doi.org/10.1126/sciadv.1601314.
[4] J. Kim, I. Jeerapan, J.R. Sempionatto, A. Barfidokht, R.K. Mishra, A.S. Campbell, L.J. Hubble, J. Wang, Acc. Chem. Res. 51 (2018) 2820–2828, https://doi.org/10.1021/acs.accounts.8b00451.
[5] D.R. Thévenot, K. Toth, R.A. Durst, G.S. Wilson, Biosens. Bioelectron. 16 (2001) 121–131, https://doi.org/10.1016/S0956-5663(01)00115-4.
[6] A. García-Miranda Ferrari, S.J. Rowley-Neale, C.E. Banks, Talanta Open 3 (2021) 100032, https://doi.org/10.1016/j.talo.2021.100032.
[7] P. Fanjul-Bolado, D. Hernández-Santos, P.J. Lamas-Ardisana, A. Martín-Pernía, A. Costa-García, Electrochim. Acta 53 (2008) 3635–3642, https://doi.org/10.1016/j.electacta.2007.12.044.
[8] J.R. Sempionatto, J.-M. Moon, J. Wang, ACS Sens. 6 (2021) 1875–1883, https://doi.org/10.1021/acssensors.1c00139.
[9] G. Cui, J.H. Yoo, J.S. Lee, J. Yoo, J.H. Uhm, G.S. Cha, H. Nam, Analyst 126 (2001) 1399–1403, https://doi.org/10.1039/B102934G.
[10] M.I. González-Sánchez, B. Gómez-Monedero, J. Agrisuelas, J. Iniesta, E. Valero, Electrochem. Commun. 91 (2018) 36–40, https://doi.org/10.1016/j.elecom.2018.05.002.
[11] D. Talarico, F. Arduini, S. Cinti, A. Amine, D. Moscone, G. Palleschi, 2015 XVIII AISEM Annual Conference, 2015, pp. 1–4, https://doi.org/10.1109/AISEM.2015.7066810.
[12] A. Muhammad, R. Hajian, N.A. Yusof, N. Shams, J. Abdullah, P.M. Woi, H. Garmestani, RSC Adv. 8 (2018) 2714–2722, https://doi.org/10.1039/C7RA07544H.
[13] X. Wang, Y. Wang, Y. Shan, M. Jiang, X. Jin, M. Gong, J. Xu, J. Electroanal. Chem. 823 (2018) 368–377, https://doi.org/10.1016/j.jelechem.2018.06.030.
[14] M. Roushani, Z. Jalilian, A. Nezhadali, Heliyon 5 (2019), e01984, https://

doi.org/10.1016/j.heliyon.2019.e01984.
[15] Y. Xiao, F. Patolsky, E. Katz, J.F. Hainfeld, I. Willner, Science 299 (2003) 1877, https://doi.org/10.1126/science.1080664.
[16] P.H.M. Hoet, I. Brüske-Hohlfeld, O.V. Salata, J. Nanobiotechnol. 2 (2004) 12, https://doi.org/10.1186/1477-3155-2-12.
[17] R.A. Yokel, R.C. MacPhail, J. Occup. Med. Toxicol. 6 (2011) 7, https://doi.org/10.1186/1745-6673-6-7.
[18] M.A. Komkova, E.E. Karyakina, A.A. Karyakin, Anal. Chem. 89 (2017) 6290–6294, https://doi.org/10.1021/acs.analchem.7b01142.
[19] A.J. Bandodkar, W. Jia, C. Yardımcı, X. Wang, J. Ramirez, J. Wang, Anal. Chem. 87 (2015) 394–398, https://doi.org/10.1021/ac504300n.
[20] F.A. Armstrong, R. Camba, H.A. Heering, J. Hirst, L.J.C. Jeuken, A.K. Jones, C. Léger, J.P. McEvoy, Faraday Discuss. 116 (2000) 191–203, https://doi.org/10.1039/B002290J.
[21] E. Laviron, J. Electroanal. Chem. Interfacial Electrochem. 101 (1979) 19–28, https://doi.org/10.1016/S0022-0728(79)80075-3.
[22] R.O. Kadara, N. Jenkinson, C.E. Banks, Sensor. Actuator. B Chem. 138 (2009) 556–562, https://doi.org/10.1016/j.snb.2009.01.044.
[23] B.-A. Mei, O. Munteshari, J. Lau, B. Dunn, L. Pilon, J. Phys. Chem. C 122 (2018) 194–206, https://doi.org/10.1021/acs.jpcc.7b10582.
[24] J. Clark, Y. Chen, S.R.P. Silva, Electroanalysis 28 (2016) 58–62, https://doi.org/10.1002/elan.201500480.
[25] L. Yue, W. Li, F. Sun, L. Zhao, L. Xing, Carbon 48 (2010) 3079–3090, https://doi.org/10.1016/j.carbon.2010.04.044.
[26] M.A. Komkova, E.E. Karyakina, A.A. Karyakin, J. Am. Chem. Soc. 140 (2018) 11302–11307, https://doi.org/10.1021/jacs.8b05223.
[27] T. Yamashita, P. Hayes, Appl. Surf. Sci. 254 (2008) 2441–2449, https://doi.org/10.1016/j.apsusc.2007.09.063.